Modelling and Simulation of Hybrid Boosting Converter for Fuel Cell Applications

A. S. Veerendra[1,2(✉)], K. Lakshmi[1,2], A. Ramesh[1,2], Ch. Punya Sekhar[3], U. P. Kumar Chaturvedula[1,2], M. Ravindra[1,2], and D. Tata Rao[1,2]

[1] Department of Electrical and Electronics Engineering, Aditya College of Engineering, Surampalem, India
veerendraump@gmail.com
[2] Jawaharlal Nehru Technological University Kakinada, East Godavari District, Kakinada, India
[3] Electrical and Electronics Engineering, Acharya Nagarjuna University, Guntur, India

Abstract. It is appropriate to focus on sustainable energy vehicles, with an intention to meet the 2050 target of an 80% reduction in greenhouse gas emissions. Fuel cells (FCs) are the only acceptable source of efficiency available in vehicles from renewable sources. Moreover, the voltage of the FC is very low to match the DC bus, which is, used to drive the motor inverter. Hence to enhance the response of the FC and to afford the desired voltage of the motor inverter, a hybrid boost converter (HBC) is suggested to give the required voltage response, as well as reduce the component stress and achieve a low output ripple. The novel topology is modeled and evaluated by using MATLAB/Simulink Software.

Keywords: hybrid boosting converter (HBC) · Sustainable energy · Fuel cell · DC-DC converter

1 Introduction

High gain dc-dc converters are the key component of the renewable energy based applications [1, 2]. Figure 1 indicates an example where the high-level converter can be used in the energy conversion phase in two phases of the system [3]. Among the various types of dc-dc converters, the non-isolated converters achieve high voltage gain than the isolated converters due to its reduced switching losses, conduction losses and absence of the transformer [4–6]. Ilango et al. [7], suggested a cascaded boost converter with high voltage and efficiency. Nonetheless, this topology has a major drawback of high cost and complexity in controller owing to the use of multiple converters. Starzyk et al. [8], proposed a dc-dc converter based on voltage multipliers. The major drawback of this topology are high conductive losses and requirement of high duty cycle. Chen et al. [9] and Muhammad et al. [10], discussed the topologies based on coupled inductors. However, these topologies needs high voltage switches and anguish from EMI problems.

Cao et al. [11], proposed a topology based on switched-capacitor for increasing the pulsating current. Nonetheless, this topology suffers with regulation problems. Zhang et al. [12], suggested a topology with a single switch for enhancing the voltage gain.

V. E. Balas et al. (Eds.): AITEES 2022, AHIS 3, pp. 33–47, 2023.
https://doi.org/10.2991/978-94-6463-074-9_5

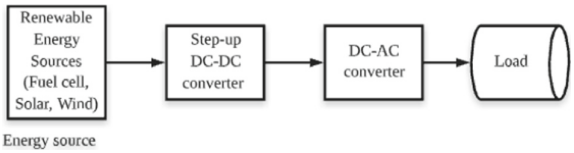

Fig. 1. Dual stage power conversion

The major obstacle of this topology is high component count in the circuit and high complexity. Later, Yao et al. [13] has reported a topology based on tapped inductor. Nevertheless, this topology needs snubbers circuits to control the leakage issues leads to increase the cost as well. Haji et al. [14] has proposed a Z-source converter topology basing on increment of switched capacitors and inductors. However, this topology suffers with high input current ripples. Da silva et al. [15] and Yang et al. [16] has suggested the topologies based on the multiple switched capacitors and inductors for increasing the voltage. The major drawback of this topology, needs high conversion ratio makes the system high complex and high cost. Hu and Gong [17] has proposed a topology based on inductors/capacitors. The major drawback of this topology is owing to its power losses of the switches. Later, Prabhakaran et al. [18] and Li et al. [19] has discussed on interleaved dc-dc converters for different applications. Nonetheless, the high component count and voltage stress of the switches are the major problem of this topology. Alternatively, the interleaved forward-flyback converter has proposed in [20]. The major limitation of this topology are reduced voltage gain and high voltage stress on the switches.

Wu et al. [21] has proposed a topology based on bipolar voltage multiplier (BVM). However, the excess component count and high complexity are the major limitations of this topology. Besides, central source multi-level boost converter suggested in [22] has a lower ripple response and a higher consumption rate for the conversion ratio of the components. In addition, some interleaving technologies have been conveyed in the literature [3, 23] for reduction and expansion of the power, but these methods are usually based on more components that are required to expand the circuit branch. Substantially more topologies permit accomplished wider voltage gains. Recently, it was also reported in [24–26], by having more components, makes it difficult in designing the circuit and it increases the cost.

Based on literature survey and pattern search, inspired by the topologies mentioned above, in this paper a hybrid boosting converter with a single inductor and a single switch with a smaller ripple while keeping up a high voltage gain is proposed. The intended converter has less component count as well as reduced total harmonic distortions (THD) with respect to voltage and current for the fuel cell (FC) system as a source.

2 Hybrid Boosting Converter (HBC)

The proposed hybrid boosting converter displayed in Fig. 2 [21], has a higher component utilization rate with respect to the same voltage gain, by integrating the input source as part of the output voltage. In this topology the interleaving operation depends on a single switch, inductor, and the input source represented as three terminal switching core.

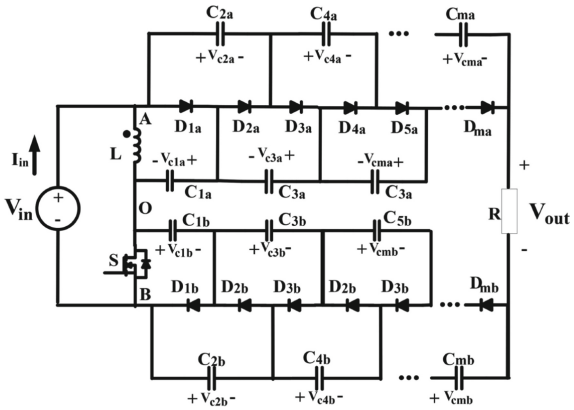

Fig. 2. General Hybrid boost converter

3 Bipolar Voltage Multiplier (BVM)

From Fig. 3(a) and (b), a BVM consists of positive and negative multipliers respectively. The positive multiplier branch is identical to the traditional voltage multiplier. The negative branch of the multiplier has the input source at the cathode terminal of the cascaded diode as shown in Fig. 3(b). The positive multiplier even-order operating modes displayed in Fig. 4 as follows; here the duty cycle is considered as D.

1) Mode 1(0, DTs): Where diodes D_{ia} (i = 2k − 1, 2k − 3, 1) from the Fig. 4(a) there are K substances produced if it is having high voltage at port AO. During this time interval, Capacitor C_{ia} (i = 2, 4… 2k) is discharged.

$$V_{c1a} = V_{AO+} \tag{1}$$

$$V_{cia} = V_{c(i+1)a} (i = 2, 4, 6, \ldots, 2k - 2) \tag{2}$$

2) Mode 2(DTs, Ts): If the voltage moves to a low level at port AO, first diode D_{2ka} is performed, shown as Fig. 4(b). Therefore the diodes D_{ia} (i = 2, 4,…) will be switched from high to low one after another. As soon as the previous one is blocked, each diode will then be turned on. The Load current is present throughout the interval of time. Although diodes all are not controlled simultaneously. The end-time interval of the flying capacitor has the relationship as below:

$$V_{c2a} = V_{c1a} - V_{AO-} \tag{3}$$

$$V_{Cia} = V_{c(i+1)a} (i = 3, 5, 7 \ldots, 2k - 1) \tag{4}$$

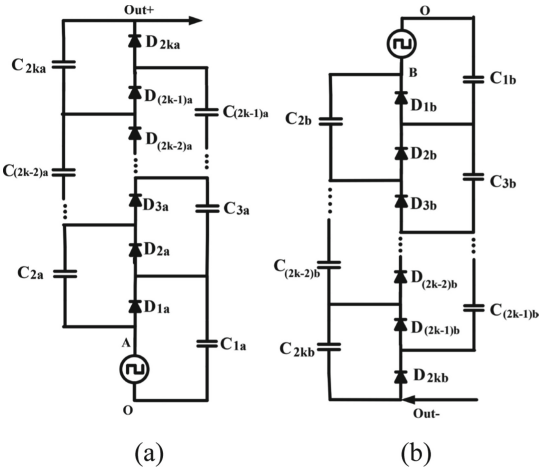

Fig. 3. (a) Bipolar Positive voltage multiplier. (b) Bipolar Negative voltage Multiplier

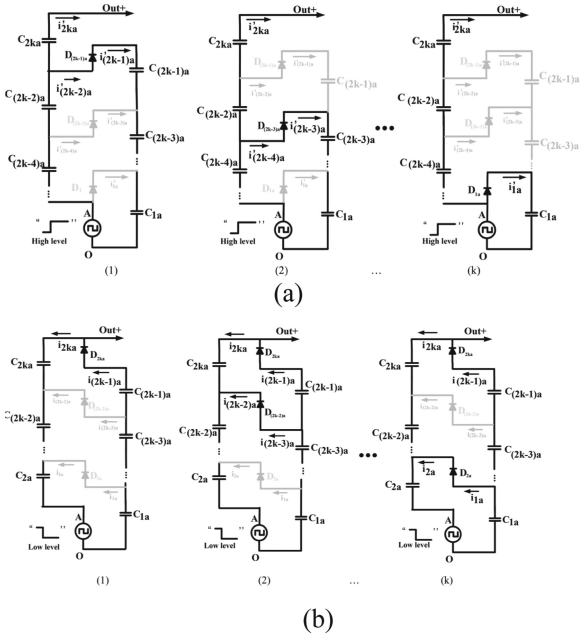

Fig. 4. Even-order positive multiplier operation a) state 1 b) state 2

Let the amount of current flowing into capacitors $C_{ia} = (2, 4\ldots 2K)$ be equal to the leaving current, in a steady-state during the switching period, based on charge balance fundamental.

$$\sum_{i=1}^{k} \int_{0}^{DTs} i'_{2ia}\, dt = \sum_{i=1}^{k} \int_{DTs}^{Ts} i_{2ia}\, dt \tag{5}$$

Accordingly, the C_{ia} capacitor group (i = 2, 4… 2k) can be substituted by a corresponding $C_{2a(eq)}$ capacitor. The D_{ia} group (i = 2, 4,… 2k) provides the $C_{2a(eq)}$ charging path which corresponds to a single $C_{2a(eq)}$ diode. Similarly, the C_{ia} (i = 1, 3,… 2k − 1) capacitor group can be interchanged with an equivalent $C_{1a(eq)}$ capacitor and D_{ia} group by $D_{1a(eq)}$. Figure 5(a) gives the branch of the positive multiplier equivalent. Basing on the same procedure, the negative branch of multipliers is equivalent as shown in Fig. 5(b).

The voltage of $C_{1a(eq)}$, $C_{2a(eq)}$ equivalent capacitors can be expressed as follows

$$V_{c2a(eq)} = K\left(V_{AO^+} - V_{AO^-}\right) \tag{6}$$

$$V_{C1a} = (K-1)\left(V_{AO^+} - V_{AO^-}\right) + V_{AO^+} \tag{7}$$

From the Fig. 5(b) negative branch, it is possible to obtain the following results based on similar analyses

$$V_{c2b(eq)} = K\left(V_{OB^+} - V_{OB^-}\right) \tag{8}$$

$$V_{C1b(eq)} = (K-1)\left(V_{OB^+} - V_{OB^+}\right) + V_{OB^+} \tag{9}$$

3) Equivalent Capacitance Derivation: In deriving the equivalent capacitance of $C_{2a(eq)}$ and $C_{1a(eq)}$, where capacitors have the same capacitance C_m, hence it is assumed that C_{ia} (i = 1, 2, 3,… 2k). To denote the flying capacitor peak-to-peak voltage ripple

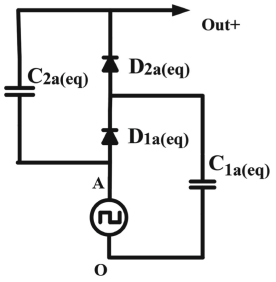

Fig. 5(a). Even-order positive multiplier Equivalent circuit

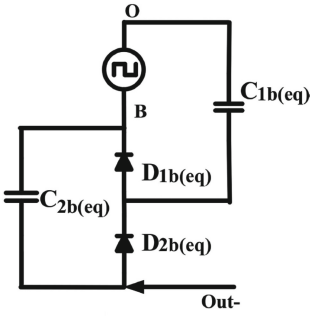

Fig. 5(b). Even-order negative multiplier Equivalent circuit

can be as good as ΔV_{Cia} (i = 1, 2, 3,… 2k), the ripple of the equivalent capacitor $C_{2a(eq)}$ may be estimated as follows

$$\Delta V = \Delta V_{c2a} + \Delta V_{c4a} + \ldots \Delta V_{c2ka} \tag{10}$$

$$\overline{i'_{ia(on)}} DT_s = \overline{i_{ia(off)}} D'T_s (i = 2, 4, \ldots 2k) \tag{11}$$

Simultaneously, state 1 provides

$$\overline{i_{ia(off)}} = \overline{i_{(i+1)a(off)}} (i = 1, 3, \ldots 2k - 3) \tag{12}$$

Similarly, State 2 provides

$$\overline{i_{ia(off)}} = \overline{i_{(i+1)a(off)}} (i = 1, 3, \ldots 2k - 3) \tag{13}$$

The subsequent correlation can be achieved on the basis of (11)–(13)

$$\begin{aligned} \overline{i_{2a(off)}} &= \overline{i_{4a(off)}} = \ldots \overline{i_{(2k-4)a(off)}} \\ &= \overline{i_{(2k-2)a(off)}} = \overline{i_{(2k-1)a(off)}} \end{aligned} \tag{14}$$

Based on the capacitor C_{2ka} load balance, the above relation derived as

$$\overline{i_{2(k-1)a(off)}} D'T_s = I_O T_s \tag{15}$$

$$\overline{i_{2ka(off)}} D'T_s = \overline{i'_{2ka(on)}} DT_s = I_O DT_s \tag{16}$$

where;

$$I_O = \frac{V_{out}}{R}$$

According to Kirchhoff's Current Law in Fig. 3(b), capacitor ripple voltage C_{ia} (I = 2, 4… 2k)

$$\begin{cases} C\Delta V_{c2a} = \overline{(i_{2ka(off)}} + \overline{i_{2k-2a(off)}} + \ldots \overline{i_{4a(off)}} + \overline{i_{2a(off)}}) D'T_s \\ C\Delta V_{c4a} = \overline{(i_{2ka(off)}} + \overline{i_{2k-2a(off)}} + \ldots \overline{i_{4a(off)}} D'T_s \\ \ldots \\ C\Delta V_{c2ka} = \overline{(i_{2ka(off)}} D'T_s \end{cases} \tag{17}$$

where

$$D' = 1 - D$$

Here, (18) can be altered to the below equation on the basis of the equations from (15) to (17):

$$\begin{cases} C\Delta V_{c2a} = (k - 1 + D) I_O T_s \\ C\Delta V_{c4a} = (k - 2 + D) I_O T_s \\ \ldots \\ C\Delta V_{c2ka} = (0 + D) I_O T_s \end{cases} \tag{18}$$

Substituting (10) to (18), the resultant is as follows,

$$C\Delta V = \left(\frac{k(k-1)}{2} + KD\right) I_O T_s \tag{19}$$

In the meantime, the following equation can be taken from an equivalent capacitor $C_{2a(eq)}$ discharge stage.

$$C_{2a(eq)}\Delta V = I_O D T_s \tag{20}$$

The corresponding capacitor $C_{2a(eq)}$ can be expressed on the basis of (19) and (20).

$$C_{2a(eq)} = \frac{2D}{k(k-1+2D)} C \tag{21}$$

4 Principle Operation of Hybrid Boosting Converter

With the reference to basic even-order Hybrid Boost Converter examination in the earlier sections, it shows that the active switch S operation intertwines the two "boost" like sub-circuits. HBC's total $V_o = V_o + V_{in}$ of two boost sub circuits, where (V_o = output voltage, V_{in} = input voltage).

1) State 1(0, DTs): Switch S is switched on in Fig. 6(a) and $D_{1a(eq)}$, $D_{2b(eq)}$ diodes are conducted while $D_{2a(eq)}$ and $D_{1b(eq)}$ diodes are biased reversely. The source of input charges the inductor L. Meanwhile, input source is utilized to charge capacitor $C_{1a(eq)}$ and capacitor $C_{2b(eq)}$ is charged by capacitor $C_{1b(eq)}$. The inductive switching core analysis is the key principle to the occurrence of the following equations.

$$V_{AO+} = V_{in} \tag{22}$$

$$V_{OB-} = 0 \tag{23}$$

2) State 2(DTs, (D+D_1) TS): In Fig. 6(b), when Switch S is off, the inductor current will be released through diodes $D_{2a(eq)}$ and $D_{1b(eq)}$. Two charging boost loops will share the inductor. In the above loop, capacitor $C_{1a(eq)}$ releases and simultaneously loads energy to capacitor $C_{2a(eq)}$. In the bottom loop, through the inductor L, the capacitor $C_{1b(eq)}$ is charged by the input source. At AO and OB, the voltage generated is expressed as follows, during this time interval based on the main inductor balance is as follows

$$V_{AO+} = V_{in} \tag{24}$$

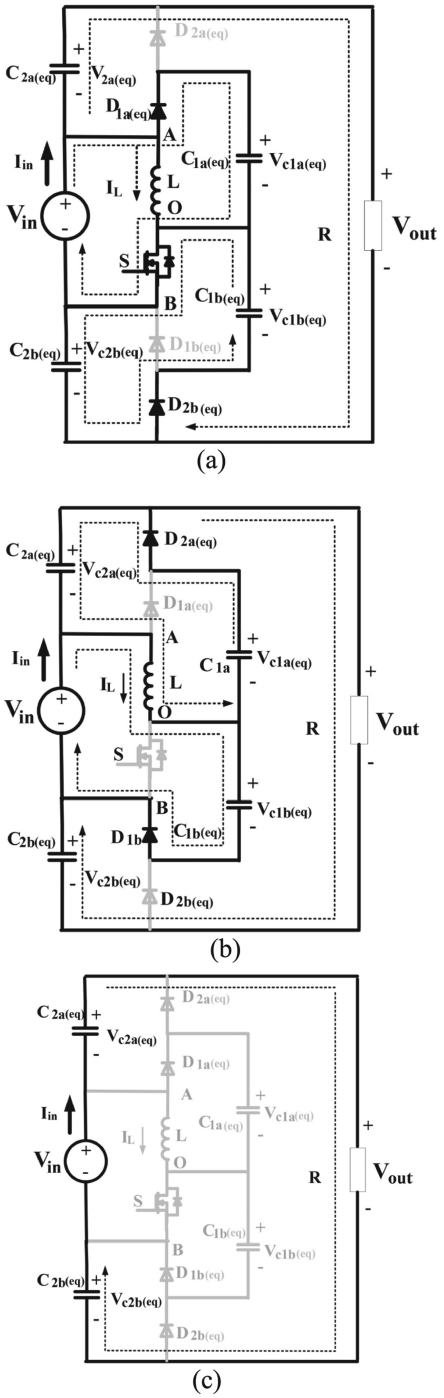

Fig. 6. HBC - (a) Operation State 1 (b) Operation State 2 (c) Operation State 3

From Fig. 7 during continuous conduction mode (CCM) the corresponding voltages of capacitors are as follows

$$V_{c2b(eq)} = K\frac{V_{in}}{D'} \tag{25}$$

$$V_{c2a(eq)} = K\frac{V_{in}}{D} \tag{26}$$

$$\frac{V_{out}}{V_{in}} = 1 + 2K\frac{1}{D'} \tag{27}$$

The average power balance is used to deduce CCM boundary conditions

$$V_{in}\left(\left(\overline{I_L}\right) + \overline{I_{D1a(eq)}}\right) = V_{out}I_O \tag{28}$$

where $\overline{I_{D1a(eq)}} = I_O = \frac{V_{out}}{R}$.

The average I_L current under CCM is therefore

$$\overline{I_L} = \frac{2K}{D'}\frac{V_{out}}{R} \tag{29}$$

Table 1. Fuel cell Simulink specifications

Parameters	Ratings
PEMFC model	50 kW–625 V DC
Number of cells	900
Operating temperature	65
Nominal operating point	[80 625]
Maximum operating point	[280 430]

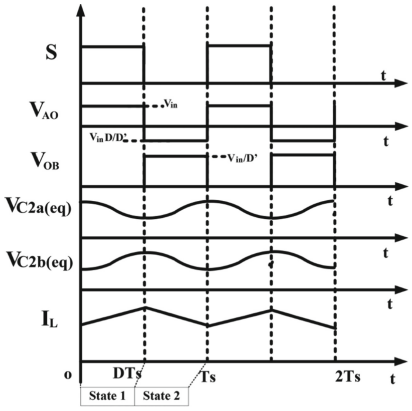

Fig. 7. Model waveforms in CCM

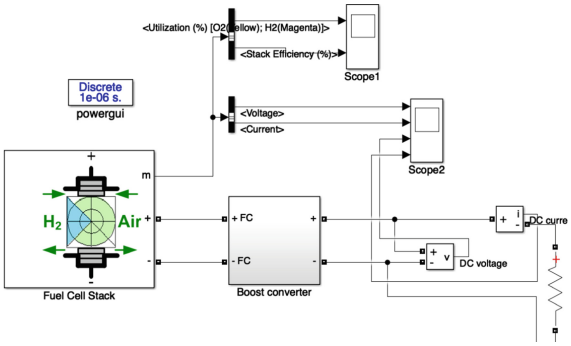

Fig. 8. Hybrid boost converter-based Fuel cell Simulink diagram.

where D is the duty cycle and K is the substates.

The inductor ripple current is

$$\Delta i_L = \frac{V_{in}}{2L} \mathrm{DT_S} \tag{30}$$

Thus, the Continuous Conduction Mode condition is

$$\frac{2K}{D'} \frac{V_{out}}{R} > \frac{V_{in}}{2L} \mathrm{DT_s} \tag{31}$$

The criteria can be rearranged as

$$\frac{2L}{RT_s} > \frac{DD'^2}{2k(D'+2k)} = K_{crit}(D) \tag{32}$$

From Fig. 8, the fuel cell acts as an input source for a proposed hybrid boost converter, having the specifications as mentioned in Table 1.

5 MATLAB/Simulink Results

In Fig. 9, a closed-loop control of Hybrid boost converter with PI controller is used to increase the voltage gain of fuel cell, here the response of the proposed converter has to attain the desired value, in which, if an error occurs, it will assist the PI controller to maintain required pulses for the switch in a closed-loop operation. The specifications are displayed in Table 2 as follows.

As per the specifications mentioned in Table 2, the corresponding input and output responses of HBC and a fuel cell in terms of stack efficiency and utilization of hydrogen is shown in Fig. 10(a) and 10(b). It is observed that the owing to its large time scale shown in graph, the input current response seems to be minute.

When the capacitance of C_{1a} is in a discharging mode, to charge the C_{2a}, during this interval C_{1b} is being charged and C_{2b} is being discharged, where C_{1b} charging

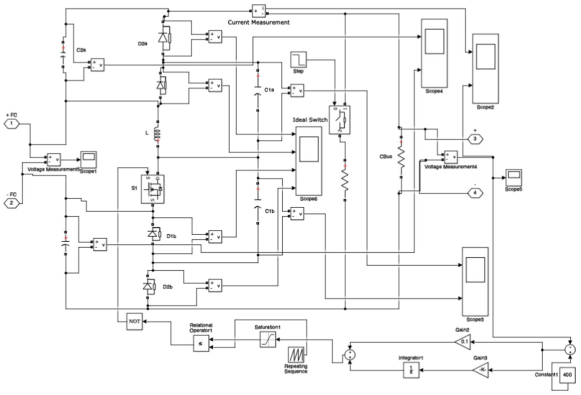

Fig. 9. Closed loop Hybrid boost converter Simulink

Table 2. Ratings of the components

Devices	Parameters	Ratings
MOSEFT	S	250 V/40 A, 29 mΩ
Inductor	L	500 μH
Diode	$(D_{1a}, D_{2a}, D_{1b}, D_{2b})$	200 V/20 A, VF = 0.78
Capacitor	$(C_{1a}, C_{2a}, C_{1b}, C_{2b})$	200 V/100 μF, *electrolytic capacitor*
Switching frequency	F_S	40 kHz
Load	R	722 Ω

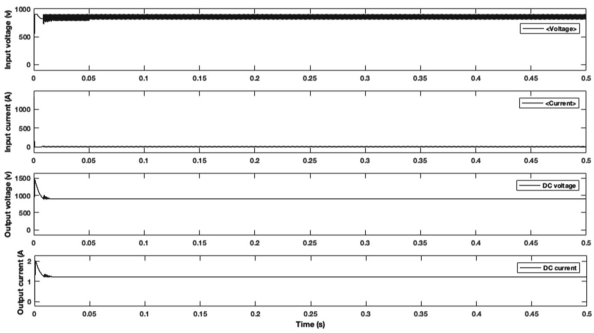

Fig. 10(a). Response waveforms of fuel cell-based hybrid boost converter.

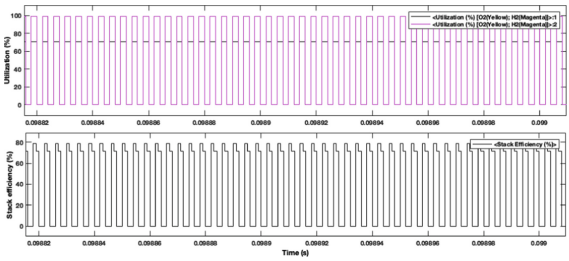

Fig. 10(b). Response waveforms of fuel cell stack.

Table 3. Hybrid boost converter comparison with other converters

Converters	Voltage gain	Diodes	Capacitors	$M_{stress} = \frac{V_{stress}}{Vout}$	$M_{ripple} = \frac{\Delta Vout}{\frac{VoutTs}{RC}}$
Boost + Dickson multiplier [17]	$\frac{3}{1-D}$	5	5	1/3	D
Boost + Cockcroft Walton multiplier [17]	$\frac{3}{1-D}$	5	5	1/3	3 + 3D
Super-lift converter [27]	$\frac{3-D}{1-D}$	4	4	1/(3 – D)	D
Multilevel boost converter [23]	$\frac{3}{1-D}$	5	5	1/3	3D
Cuk-derived converter [21]	$-\frac{2}{1-D}$	3	3	1/2	1 − D
Modified voltage lift converter [3]	$\frac{2}{1-D}$	3	3	1/2	D
Hybrid boost converter	$\frac{3-D}{1-D}$	4	4	1/(3 – D)	|2D − 1|

corresponds to the input voltage. The corresponding responses of the capacitances are presented i.e., is C_{1a} an C_{1b} in Fig. 10(c); C_{2a} and C_{2b} voltages respectively in Fig. 10(d).

In Table 3, a comparison is made among the previous and proposed converter. It is noted that the suggested converter has the lowest stress voltage of a capacitor with a duty cycle of 0.5 and 0.8 compared to other converters from Eqs. (8) and (19). From Eq. (20) and (22) the output ripple can be measured seems to be very low compared to other converters. It has high-power density and low-cost design compared to previous converters. Nevertheless, as with most of the previous converters had improved the voltage gain with a greater number of components, hence the proposed converter can be employed, as it has lowered the stress voltage of a capacitor, has a high-power density and low cost owing to its low usage of components.

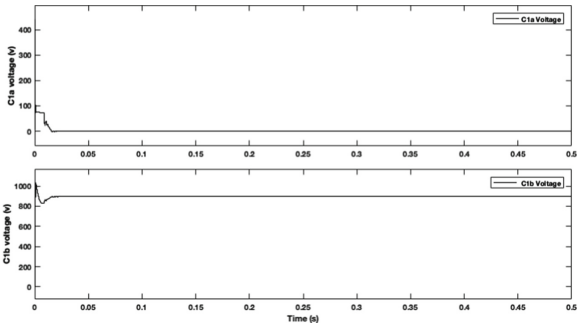

Fig. 10(c). Responses of C_{1a} and C_{1b} capacitors in hybrid boost converter

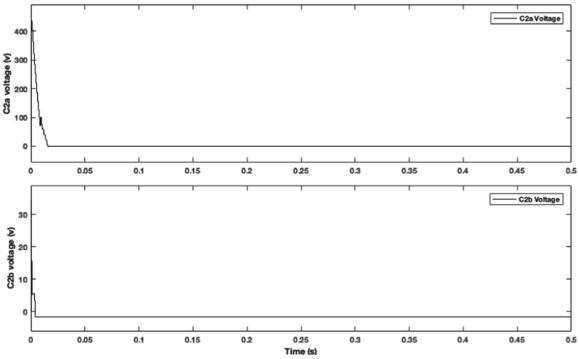

Fig. 10(d). Responses of C_{2a} and C_{2b} capacitors in hybrid boost converter

6 Conclusion

This paper proposes a closed-loop control of hybrid boosting converter for a voltage gain of 50 kW–625 V fuel cell stacks with Mutual benefits, Capacity for regulation from its Strengthening structure and improvement of multiplier voltage. The novel converter includes a bipolar voltage multiplier with high gain capability with broad regulatory range, reduced component stress, making it suitable for applications in fuel cells. This paper analyzes the main operation; component stress and output ripple and compares its voltage gain with conventional topologies, makes this topology suitable for mass production.

Acknowledgments. This work was supported by Aditya College of Engineering.

Authors' Contributions. **A. S. Veerendra:** Conceptualization, methodology, validation, writing original draft. **K. Lakshmi:** Supervision, visualization, validation. **A. Ramesh:** Supervision, Review. **Ch. Punya Sekhar:** Software, methodology. **U. P. Kumar Chaturvedula:** Review and Editing. **M. Ravindra:** Review and Editing. **D. Tata Rao:** Review and Editing.

References

1. Veerendra, A.S., Mohamed, M.R., Sulaiman, M.H., Leung, P.K.: Modeling and analysis of hybrid multilevel converter for constant DC and fuel cell sources. Energy Storage **2**(6), e193 (2020)
2. Oulad-Abbou, D., Doubabi, S., Rachid, A.: Power switch failures tolerance of a photovoltaic fed three-level boost DC-DC converter. Microelectron. Reliab. **92**, 87–95 (2019). https://doi.org/10.1016/j.microrel.2018.11.017
3. Veerendra, A.S., Mohamed, M.R., Peddakapu, K., Sekhar, C.P.: Minimization of total harmonic distortion and enhancing voltage level for hybrid multilevel converter with different sources. Adv. Control Appl. Eng. Ind. Syst. **2**(4), e58 (2020)
4. Nguyen, M.K., Duong, T.D., Lim, Y.C., Kim, Y.J.: Isolated boost DC-DC converter with three switches. IEEE Trans. Power Electron. **33**(2), 1389–1398 (2018). https://doi.org/10.1109/tpel.2017.2679029
5. Nahavandi, A., Hagh, M.T., Sharifian, M.B.B., Danyali, S.: A nonisolated multiinput multioutput DC–DC boost converter for electric vehicle applications. IEEE Trans. Power Electron. **30**(4), 1818–1835 (2015)
6. Veerendra, A.S., Mohamed, M.R., Sulaiman, M.H., Peddakapu, K.: An improved efficiency of solar photo voltaic system applications by using DC-DC zeta converter. In: ECCE2019. Lecture Notes in Electrical Engineering, vol. 632, pp. 737–751. Springer, Singapore (2020). https://doi.org/10.1007/978-981-15-2317-5_62
7. Ilango, K., Ram, S., Nair, M.G.: A hybrid photovoltaic-battery powered DC-DC converter with high conversion ratio and reduced switch stress. In: IEEE International Conference on Power Electronics, Drives and Energy Systems, Pedes 2012 (2012)
8. Starzyk, J.A., Jan, Y.W., Qiu, F.J.: A DC-DC charge pump design based on voltage doublers. IEEE Trans. Circ. Syst. I Fundam. Theor. Appl. **48**(3), 350–359 (2001). https://doi.org/10.1109/81.915390
9. Chen, Y.T., Lu, Z.X., Liang, R.H.: Analysis and design of a novel high-step-up DC/DC converter with coupled inductors. IEEE Trans. Power Electron. **33**(1), 425–436 (2018). https://doi.org/10.1109/tpel.2017.2668445
10. Muhammad, M., Armstrong, M., Elgendy, M.A.: Analysis and implementation of high-gain non-isolated DC-DC boost converter. IET Power Electron. **10**(11), 1241–1249 (2017). https://doi.org/10.1049/iet-pel.2016.0810
11. Cao, D., Peng, F.Z.: A family of zero current switching switched-capacitor dc-dc converters. In: 2010 25th Annual IEEE Applied Power Electronics Conference and Exposition (APEC), pp. 1365–1372. IEEE (2010)
12. Zhang, N., Zhang, G.D., See, K.W., Zhang, B.: A single-switch quadratic buck-boost converter with continuous input port current and continuous output port current. IEEE Trans. Power Electron. **33**(5), 4157–4166 (2018). https://doi.org/10.1109/tpel.2017.2717462
13. Yao, J., Abramovitz, A., Smedley, K.M.E.: Steep-gain bidirectional converter with a regenerative snubber. IEEE Trans. Power Electron. **30**(12), 6845–6856 (2015)
14. Haji-Esmaeili, M.M., Babaei, E., Sabahi, M.: High step-up quasi-z source DC-DC converter. IEEE Trans. Power Electron. **33**(12), 10563–10571 (2018). https://doi.org/10.1109/tpel.2018.2810884
15. da Silva, E.S., Barbosa, L.D., Vieira, J.B., de Freitas, L.C., Farias, V.J.: An improved boost PWM soft-single-switched converter with low voltage and current stresses. IEEE Trans. Industr. Electron. **48**(6), 1174–1179 (2001). https://doi.org/10.1109/41.969396
16. Yang, L.S., Liang, T.J., Chen, J.F.: Transformerless DC-DC converters with high step-up voltage gain. IEEE Trans. Industr. Electron. **56**(8), 3144–3152 (2009). https://doi.org/10.1109/tie.2009.2022512

17. Hu, X.F., Gong, C.Y.: A high voltage gain DC-DC converter integrating coupled-inductor and diode-capacitor techniques. IEEE Trans. Power Electron. **29**(2), 789–800 (2014). https://doi.org/10.1109/tpel.2013.2257870
18. Prabhakaran, P., Agarwal, V.: Novel boost-SEPIC type interleaved DC-DC converter for mitigation of voltage imbalance in a low-voltage bipolar DC microgrid. IEEE Trans. Industr. Electron. **67**(8), 6494–6504 (2020). https://doi.org/10.1109/tie.2019.2939991
19. Li, Q., et al.: An improved floating interleaved boost converter with the zero-ripple input current for fuel cell applications. IEEE Trans. Energy Convers. **34**(4), 2168–2179 (2019). https://doi.org/10.1109/tec.2019.2936416
20. Tseng, K.C., Chen, J.Z., Lin, J.T., Huang, C.C., Yen, T.H.: High step-up interleaved forward-flyback boost converter with three-winding coupled inductors. IEEE Trans. Power Electron. **30**(9), 4696–4703 (2015). https://doi.org/10.1109/tpel.2014.2364292
21. Wu, B., Li, S., Liu, Y., Smedley, K.M.: A new hybrid boosting converter for renewable energy applications. IEEE Trans. Power Electron. **31**(2), 1203–1215 (2015)
22. Rosas-Caro, J.C., Ramirez, J.M., Peng, F.Z., Valderrabano, A.: A DC-DC multilevel boost converter. IET Power Electron. **3**(1), 129–137 (2010). https://doi.org/10.1049/iet-pel.2008.0253
23. Li, W., He, X.: An interleaved winding-coupled boost converter with passive lossless clamp circuits. IEEE Trans. Power Electron. **22**(4), 1499–1507 (2007). https://doi.org/10.1109/tpel.2007.900521
24. Ismail, E.H., Al-Saffar, M.A., Sabzali, A.J., Fardoun, A.A.: High voltage gain single-switch non-isolated DC-DC converters for renewable energy applications. In: 2010 IEEE International Conference on Sustainable Energy Technologies (ICSET), pp. 1–6. IEEE (2010)
25. Zhao, Y., Xiang, X., Li, C., Gu, Y., Li, W., He, X.: Single-phase high step-up converter with improved multiplier cell suitable for half-bridge-based PV inverter system. IEEE Trans. Power Electron. **29**(6), 2807–2816 (2014)
26. Kim, J.-K., Moon, G.-W.: Derivation, analysis, and comparison of nonisolated single-switch high step-up converters with low voltage stress. IEEE Trans. Power Electron. **30**(3), 1336–1344 (2015)
27. Lamantia, A., Maranesi, P.G., Radrizzani, L.: Small-signal model of the Cockcroft-Walton voltage multiplier. IEEE Trans. Power Electron. **9**(1), 18–25 (1994). https://doi.org/10.1109/63.285489